1

FAIMS Detection Technology Based on MEMS

Fei Tang, Xiaohao Wang and Chulong Xu
Tsinghua University
Peoples Republic of China

1. Introduction

1.1 The research background of FAIMS

To build a resource-conserving and environmentally friendly society is a strategic mission in the long-term plan of a national economy and society development. Environmental protection regulation, is not only about preventing pollution and protecting ecosystem, but also includes the fast detection of environmental pollutants. Thus, analytical apparatus for the fast and effective detection of environmental pollutants is required. Besides, the real-time detection technology of the trace amounts of chemicals, drug, explosive material, etc. is also an important technical method to maintain people's health, social stability and national security.

At present, common detection methods use complex, expensive and bulky detection equipment or have complex procedures without portability, which limits their use. For example, methods like mass spectrometry, atomic fluorescence and so on need complex instruments. In contrast, titration and colorimetry only need simple equipment, but their process of operation is complex, which leads to time-consuming, low efficiency and highly demanding operations. So these kinds of methods are hard to promote.

With the increasing demand in application, portable and low power consuming micro-chemical analysis detection instruments are urgently required. Ion Mobility Spectrometry (IMS), which plays a very important role in the detection of explosive substances, poison and chemical warfare agents, etc., was developed during the 1970s. In IMS, substances are separated mainly according to differences in the mobility of ions under low electric fields in order to analyse each kind of the substance. Up until now, many kinds of commercial IMS have appeared, which have been widely used in detection of the environmental pollutants, explosive materials, drug and chemical warfare agents, etc. (West et al., 2007; Laiko et al., 2006; Borsdorf et al., 2006). The drift tube of IMS is a metal ring structure, which is adverse to miniaturisation (Miller et al., 2001). In the high-field asymmetric waveform ion mobility spectrometry (FAIMS) developed in recent years, the drift tube is a flat plate structure, which makes it easy to fabricate with Micro Electro Mechanical Systems (MEMS). It has many strengths, such as miniature size, high sensitivity, short test time, numerous test substances, low power usage, etc. So it can be used to detect substances instead of IMS. In addition, substances of same or similar ion mobility under the conditions of the low electric field which are hard to separate in IMS, can be separated by the difference in the ion mobility in the high electric field of FAIMS (Miller et al., 2000). On the other hand, FAIMS can be used together with a mass spectrograph, and can bring ion filtration and selection to the mass spectrograph, resulting in decreased background noise and improved signal to

noise ratio (Barnett et al., 2002). In conclusion, wide prospects for the FAIMS sensor based on MEMS technology exist, which can bring huge social and economic benefits.

1.2 Current status and developing trend of FAIMS technology

Since the 1990s, The Canadian Institute for National Measurement Standards, New Mexico State University of the USA, Sionex company, Pacific Northwest National Laboratory, Owlstone Company of the UK, Thermo Company of the US, etc. have all developed sensors with the FAIMS principle, one after another (Guevremont et al., 1999; Eiceman et al., 2000; Nazarov et al., 2006; Shvartsburg et al., 2004; Barnett et al., 2007), in which the New Mexico State University, Sionex company and the Owlstone Company are leading the miniaturisation of the FAIMS sensors with MEMS technology (Miller et al., 2001; Eiceman et al., 2001; Shvartsburg et al., 2009).

Eiceman, etc. from the New Mexico State University developed a small ion filter based on the principle of FAIMS with MEMS technology, with which toluene with a detection limit of up to 100ppb can be measured. This device is composed by a $3\times1\times0.5cm^3$ rectangular drift tube and a set of parallel plate electrodes. The size of the whole chip is just like a coin. Figure 1 shows the chip of the FAIMS detector made by Eiceman (Miller et al., 2001).

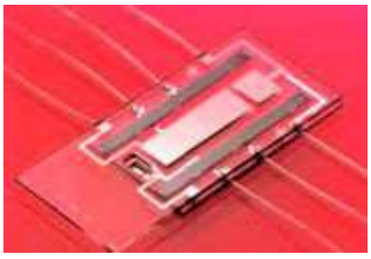

Fig. 1. Micro FAIMS detector

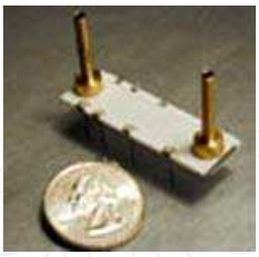

Fig. 2. MicroDMx™ chip made by Sionex

Fig. 3. Commercial FAIMS product developed by the Sionex company

The Sionex Company was founded in the USA in 2000, and is mainly engaged in the research and development of mico-FAIMS detection parts, and it is leading in the utility and commercialisation of the FAIMS technology. With the technology from the Eiceman's research group of New Mexico State University and the Charles Stark Draper Laboratory, the company has developed a micro FAIMS detector. The core of its products is the microDMx™ sensor platform, as shown in figure 2 (Miller et al., 2000).

Based on the microDMx™ chip, the Sionex company has developed a commercial product, as shown in figure 3. This product has a high detection sensitivity (up to ppb), and a short detection time (from 30 seconds to 5 minutes), which can be used in anti-terrorism, process control, environmental monitoring and medical diagnosis, etc.

The Owlstone Company in the U.K. is also engaged in the research of the micro detector based on FAIMS technology. This company plans to develop a kind of chemical sensor with the size of a coin, which can be used to detect trace amounts of explosive substances. In addition, this sensor can be used in civil applications such as family fire monitoring and early disease diagnosis, etc. In the FAIMS technology of Owlstone, one small space (10 micrometre), short path (depth of a silicon chip) and a muti-channel array type of drift tube structure is used, as shown in figure 4. Compared to the traditional FAIMS structure, the multi-channel can improve the sensitivity; the small space can decrease the radio frequency voltage amplitude needed; the short path can decrease the ion travelling time in the shift tube and increase the analytical efficiency (Shvartsburg et al., 2009).

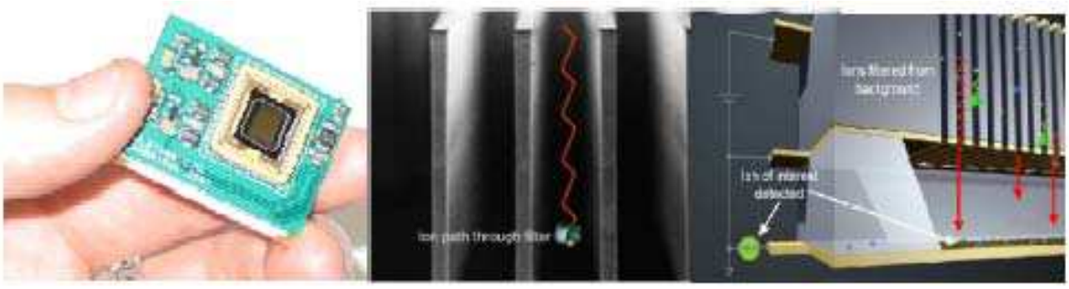

Fig. 4. FAIMS principle and chip of Owlstone Company

Based on the multi-channel FAIMS chip structure, the Owlstone Company has developed two commercial products: LONESTAR and Nexsense C, as shown in figure 5. The weight of these two products is 7.8kg and 7kg, respectively, with a built-in chargeable power supply. It can be used continuously for three hours, which is convenient for field operation.

Fig. 5. FAIMS products from the Owlstone Company. Left: LONESTAR; Right: Nexsense C

2. Principle of FAIMS

FAIMS separates different kinds of compounds mainly based on the ion mobility difference under electric field changes by varying the electric field intensity. When the electric field intensity is over a certain value (over 10000V/cm), the mobility of the ion will change non-linearly with the electric field intensity, as shown in figure 6 (Buryakov et al., 1993). Here, $K = K_0(1+\alpha)$, where K is the mobility of the ion in the high electric field; K_0 is the mobility of the ion in the low electric field; α is the efficiency coefficient of the ion mobility, which is different for different kinds of ion.

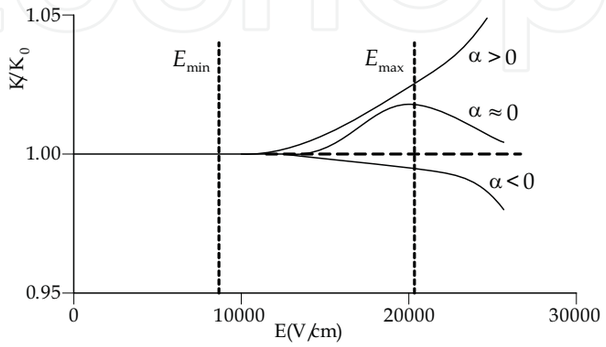

Fig. 6. Relation between ion mobility and the electric field intensity in three cases

In figure 6, we can see that the change of mobility for ions A, B and C is different in the high electric field. The mobility of ion A will increase with an increase in the electric field intensity; when the electric field intensity increases, the mobility of ion B will primarily increase and then decrease; while the mobility of ion C will decrease when the electric field intensity increases. In general, the ions with small mass-to-charge ratio m/z (m/z is less than 300) belong to the A type of ion; while ions with a large mass-to-charge ratio m/z (m/z is greater than 300) belong to the C type of ion. The change in mobility when the electric field intensity changes is related to the size of the ion, interaction between ion and molecule, and the structural rigidity of the ion.

In conclusion, when the electric field intensity is greater than 10000V/cm, the ion mobility will have a different non-linear changing trend, so that an ion with the same or similar mobility in the low electric field intensity can be separated under the influence of the high electric field intensity. The change in ion mobility under the influence of the high electric field intensity is also related to the gas concentration. The variation range of K with the electric field is defined by E/N, in which E is the electric field intensity and N is the gas density, namely the number of the gas molecule in unit volume. The unit of E/N is Townsend (Td). It is presumed that the electric field intensity is 1000V/cm, under the condition of one atm and 273K, the gas density N will be 2.7×10^{19}, so the value of E/N is about 3.7×10^{-17}. It is defined that 1Td is equal to 1×10^{-17}, and the value of E/N is about 3.7Td under the above conditions. When the value of E/N is about 40Td, the ion mobility begins to change when the electric field intensity increases. Under high electric field intensity, the relation between the ion mobility K and the electric field intensity is shown as follows (Krylov et al., 2003):

$$K = K_0[1 + \alpha_1(E/N)^2 + \alpha_2(E/N)^4 + \ldots\ldots] \quad (1)$$

Formula (1) can be simplified or approximated into following formula:

$$K \approx K_0[1+\alpha(E)] \tag{2}$$

Where $\alpha(E)$ is the function of the electric field intensity. According to formula (2), when $\alpha(E)$ is above zero, K will increase as E increases; when $\alpha(E)$ is below zero, K will decrease as E increases; and when $\alpha(E)$ is near to zero, K will change slightly. These three cases correspond to the three kinds of ion in the high electric field intensity.
The expression of the asymmetrical waveform voltage used in the FAIMS is shown as follows:

$$U_d(t)=\begin{cases} U_d,(T-pT+mT\le t\le T+mT) \\ -\dfrac{pU_d}{1-p},(mT\le t\le T-pT+mT) \end{cases} \tag{3}$$

Where, m is an integer number, U_d is the amplitude value of the high voltage, p is the coefficient of the duty ratio, T is the cycle of the voltage signal. Thus its corresponding electric field is $E_d(t)=\dfrac{U_d(t)}{d}$, where d is the plate electrode space in the drift tube, the waveform of $E_d(t)$ is shown in figure 7. $E_d(t)$ must meet the following criteria:

$$10000V/cm<\left|E_{\max}\right|<30000V/cm$$
$$\left|E_{\max}\right|>>\left|E_{\min}\right|$$
$$\left|E_{\max}\right|t_1-\left|E_{\min}\right|t_2=0$$

It is supposed:

$$\left|E_{\max}\right|t_1=\left|E_{\min}\right|t_2=\beta \tag{4}$$

where, β is the random shadow's area in the figure 7, which is a constant value.

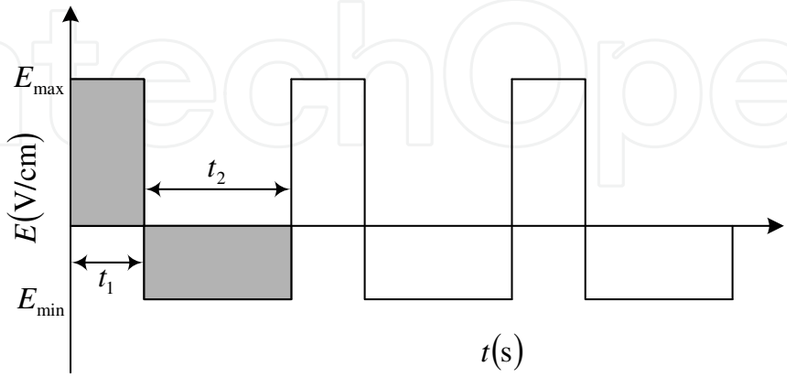

Fig. 7. Electric field of asymmetric waveform

When the high-field asymmetric waveform electric field $E_d(t)$ is applied to the narrow space formed by a pair of electrodes and the ion is brought in by the carrier gas flow, the ion

will vibrate between the two plate electrodes. Taking an ion of negative electric charge into consideration, the zigzag vibration routes when $\alpha > 0$, $\alpha \approx 0$ and $\alpha < 0$ are shown in figure 8. It can be seen that in t_1 of one vibration period, corresponding with the high electric field intensity $E_{\max}$, these three ions will move towards the upper plate of the electrode; while within t_2 of the vibration period, corresponding to the low electric field intensity $E_{\min}$, these three ions will move towards the lower plate electrode; the vibration direction is vertical to the plate electrode.

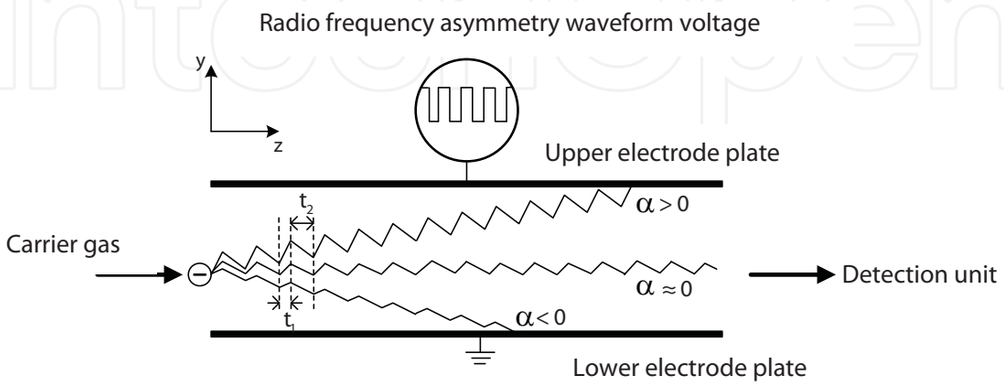

Fig. 8. Motion track of the ions in the drift tube α

During t_1 and t_2, the ion can be approximated as a uniform motion. It is supposed that the velocity of the ion during t_1 is V_1 and the velocity during t_2 is V_2. When the velocity of the ion is changed to V_2 from V_1, there is a speeding up or down, which takes time as follows (Buryakov et al., 1993):

$$\Delta t = \frac{2mV_1}{qE_{\max}} = \frac{2mK}{q} \tag{5}$$

Where, m is the mass of the ion, q is the charge of the ion, K is the mobility of the ion. The time Δt for speeding up or down of the ion is very small, so Δt can be ignored compared to the radio frequency asymmetry waveform voltage period.

The mathematical model is set up with a type A negative ion as the research object, the velocity of the ion in the Y direction is:

$$V_Y = K(E)E(t) \tag{6}$$

During t_1, the ion moves towards the upper plate electrode, the expression is as follows:

$$V_{\text{up}} = K\left|E_{\max}\right| \tag{7}$$

During t_2, the ion moves towards the lower plate electrode, the expression is as follows:

$$V_{\text{down}} = K_0\left|E_{\min}\right| \tag{8}$$

Then, the net displacement of the ion in the Y direction within a cycle:

$$\Delta Y = K\left|E_{\max}\right|t_1 - K_0\left|E_{\min}\right|t_2 \tag{9}$$

Substituting (4) into (9):

$$\Delta Y = \beta(K - K_0) = \Delta KpT \tag{10}$$

From formula (10), the net displacement ΔY of the ion in one cycle will increase when the duty ratio p or the cycle T of the asymmetry waveform radio frequency voltage increase. The average velocity of the ion within a cycle is:

$$\overline{V_Y} = \frac{\Delta Y}{t_1 + t_2} = \frac{\beta \Delta K}{T} \tag{11}$$

At the same time, the ion will move toward the detection unit along the Z direction of the drift tube driven by the carrier gas, so the total displacement in the Y direction is:

$$Y = \overline{V_Y} t_{res} \tag{12}$$

Where t_{res} is the residence time of the ion in the drift tube, which can be determined according to the following:

$$t_{res} = \frac{\mathrm{AL}}{\mathrm{Q}} \tag{13}$$

In the above formula, A is the cross sectional area of the drift tube, L is the length of the drift plate electrode, and Q is the gas flow velocity in the drift tube. So the residence time of the ion in the drift tube is proportional to the length of the drift area, and inversely proportional to the flow velocity of the gas carrier. Substitute (11) and (13) into (12), and take account of $\left|E_{\max}\right| t_1 = \beta$ in (4), if $p = \mathrm{t}_1 / T$, then:

$$Y = \frac{\Delta K E_{\max} ALp}{\mathrm{Q}} \tag{14}$$

Where Y depends on the average residence time of the ion in the drift region. It can be calculated from formula (13) that the displacement of the ion in the Y direction is in direct proportion to ΔK which is the difference in mobility between the high and low electric fields. In every cycle of the radio frequency electric field, the ion will move a net displacement towards the upper plate electrode (or the lower plate electrode). Because ΔK for different types of ions is different, there are particular motion tracks for different ions under the effect of the carrier gas and the electric field. If a DC voltage U_C acts on the electrode in the drift tube simultaneously with the RF voltage, and E_c : $\left|E_c\right| < \left|E_{\min}\right| << \left|E_{\max}\right|$, it can generate an electric field force, the direction of which is opposite to the direction of the net displacement of the ion, making the displacement of the ion in every cycle zero along the direction of the electric field and ions vibrate up and down along one right line of the Z axis. So that a specific kind of ion will be detected when it comes through the drift region between the two electrodes, instead of striking with the electrodes of the drift region. The other ions will strike the electrodes of the drift region, become neutral and then be transported out of the drift region by the carrier gas flow. Every type of ion has its specific direct current voltage, which is called compensation voltage.

From the above, it can be concluded that the drift region of the high-field asymmetric waveform ion drift spectrometer is equivalent to a filter. When the compensation voltage

U_C is set for a specific ion, only this ion can pass through, while other ions will be neutralised by the electrode and cannot pass. When U_C is swept through a certain range, all ions in the FAIMS system can be characterised, producing the FAIMS spectrogram of the ion in the carrier gas flow. In the FAIMS drift spectrogram, the longitudinal axis is the current signal intensity of the ion, and the horizontal axis is the compensation voltage.

3. Design of the ion source

3.1 Selection of the ionisation scheme

The ion source changes the neutral molecule in the sample into a charged ion, so that the substance can be detected by FAIMS. It is out of the question that the ion source is a premise for the functioning of the subsequent parts of FAIMS.

According to the operational principle and the application characteristics of FAIMS, the ion source must meet following requirements:

1. Compatibility with MEMS technology. In order to decrease the volume of the system, the FAIMS system is fabricated with MEMS technology, so the ion source should be compatible with MEMS technology.
2. Can work stably under atmospheric pressure.
3. No radioactivity.
4. Minor ion fragmenting. If one substance is ionised into many kinds of ion fragments, more ions should be filtered by the drift region, which would decrease the resolution of the system.
5. Little electromagnetic interference. If the ion source emits intense electromagnetic waves, they will affect the electric field in the drift tube, will affect the movement of ions and will interfere with the detection of the weak ion current, and finally the resolution and sensitivity of the system will also be affected.
6. Little hydration clustering. The ions will form clusters with the water molecules in the high electric field, and these clustered ions will not be stable or easy to decompose. Usually, the compensation voltages of the ion and its hydration cluster ion are different. In the drift region, the ions combine with water and then decompose repeatedly, so that the system works at improper conditions and is unable to separate ions.

The principles of corona discharge ionisation and atmospheric pressure glow discharge ionisation are similar. They are both “soft ionizing”, with minor ion fragmenting effects, mainly the molecular ion peak which is consistent with the requirements of FAIMS. Gas discharge is generated through a pair of electrodes applied with a voltage, and the electrodes can be made with highly conductive silicon in MEMS technology (Khayamian et al., 2003; Tabrizchi et al., 2004; Jafari et al., 2007; Khayamian et al., 2001). The discharge can be achieved by DC voltage. This can reduce electromagnetic interference as much as possible, and reduce the effects on the drift region and detection unit.

Therefore, corona discharge ionisation and atmospheric pressure glow discharge ionisation are more suitable for the application of the FAIMS ion source.

3.2 Corona discharge ion source

Figure 9 (a) shows the traditional line - tube structure. It can be seen from the figure that the voltage is applied on the inside and outside of the electrode, and the direction of the electric field is perpendicular to the axial direction of the inner electrode. Under the effect of the electric field force, the ions generated collide with the electrode, hence cannot come out of

the electrode. Even if there is a strong flow blowing the ion outwards along the direction of the inner electrode, the ions will also be lost due to the effect of the electric field, because of the frequent collisions of the ion and the carrier gas molecules, which can lead to a loss resulting from plasma chemical reactions. After making improvements based on this structure, the structure as shown in figure 9(b) is formed. In the improved structure, because of slots in the outer electrode, it is possible to make the sample pass over it. These slots can be achieved by the ICP or DRIE process. In this article, the electrode diameter in the line - tube structure is 0.16 mm, the diameter of the outer cylinder electrode is 4mm, and the outside diameter 6mm.

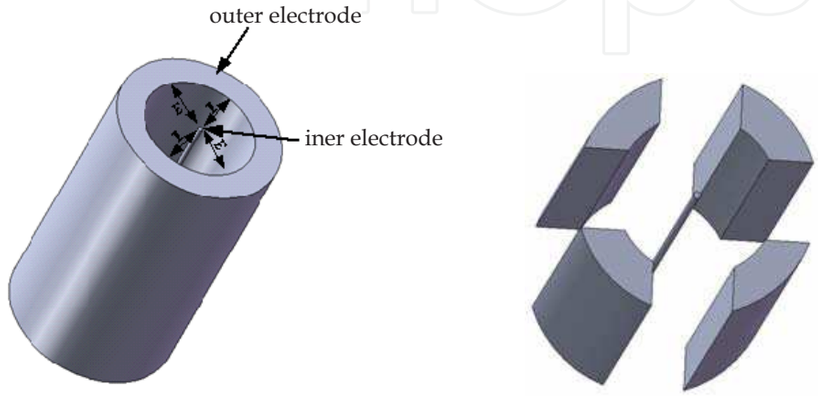

(a) (b)

Fig. 9. Line – tube structure. (a) Traditional line – tube structure; (b) Improved line – tube structure.

3.3 Ionisation characteristics of the corona discharge ion source

In this section, at the base of the stable gas discharge, we test and analyse the performance of the corona discharge ion source through the mass spectrometry experiment.
According to the chemical characteristics, the experiment is divided into two parts: one is the positive ion experiment, and the other one is the negative ion experiment.

3.3.1 Positive ion test

Figure 10 is the circuit diagram of the mass spectrometry experiment on positive ionisation mode. When the ion source works under the environmental atmospheric pressure, the average free path of the ion is very small and the ions collide frequently during movement. In order to reduce the ion loss as much as possible, the ion should be accelerated into the mass spectrograph. The voltage on the collection cone of the mass spectrometer is 80V in positive ion mode, and the voltages of the external electrode and the pulled electrode are respectively set at 200V and 150V. The voltages of the external electrode and the pulled electrode are supplied by the power supply between 0 - 500V. After the chemical substance is carried into the ion source by the carrier gas (N_2), the high voltage direct current source is turned on. When the voltage is of about 3700V, the corona discharge starts, and the chemical substance is ionised. Then the ionised ion will fly out of the external electrode driven by the electric field force and will then enter the mass spectrometer driven by the pulling electrode.

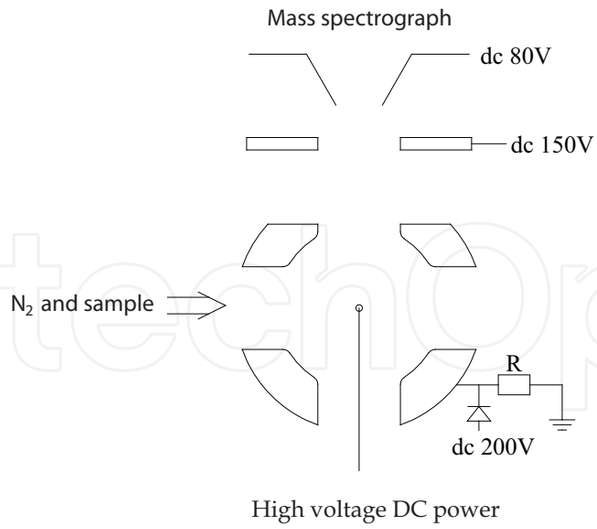

Fig. 10. Mass spectroscopic circuit diagram under the mode of positive ionisation

In this experiment, the flow velocity of the carrier gas is 100L·h^{-1} at room temperature and the sample is analytically pure without any preliminary treatment. We have carried out the ionisation experiment for acetone, N,N—dimethyl formamide, aniline, alcohol, ethyl acetate, dimethyl methyl phosphate (DMMP), methanol, acetonitrile, styrene. The results are shown in the figure 11.

For acetone, N,N—dimethyl formamide, aniline, alcohol, ethyl acetate, DMMP, methanol, acetonitrile and styrene, the experiment shows simple results and single ion peaks, they are mainly $[M+H]^+$ and dimeric ions $[M+M+H]^+$. However the ionisation results of benzyl alcohol, styrene are relatively complex. The ionisation of these substances possibly needs the participation of oxygen, so these ions are oxidised and dehydrated. The ionising result of benzyl alcohol is relatively simple with the main peak of m/z:91, which is possibly the result of dehydration after acquiring the proton. It can be expressed as $[M+H - H_2O]^+$. Main peaks in the ionising results of styrene are m/z:91 and m/z:103, which is possibly because the formaldehyde or water is lost after the styrene is oxidised. It can be expressed with $[M+O+H - CH_2O]^+$ and $[M+O+H - H_2O]^+$.

3.3.2 Negative ion experiment

The negative ionisation mode is the same as the positive ionisation mode, except that the voltage is negative. The voltage in the collection cone of the mass spectrometry is -80V, and the voltages of the external electrode and the pulled electrode are set at -200V and -150V, respectively. After the chemical substance is carried into the ion source by the carrier gas (N_2), the high voltage direct current source is turned on. When the voltage is up to about -3700V the corona discharge starts, and the chemical substance is ionised. Then the ionised ion will be boosted off the external electrode driven by the electric field force and then will enter the mass spectrometer driven by the pulling electrode.

In this experiment, the flow velocity of the carrier gas is 100 L·h^{-1} at room temperature, and the sample is analytically pure without preliminary treatment. We have carried out the ionisation experiment for formic acid, acetic acid and phenol. The results are shown in figure 12.

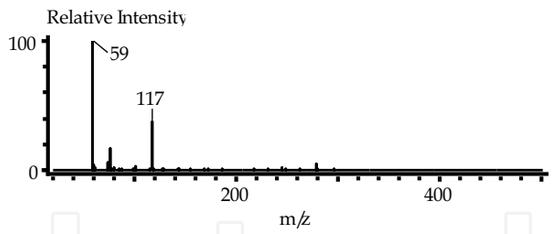

(a) Acetone

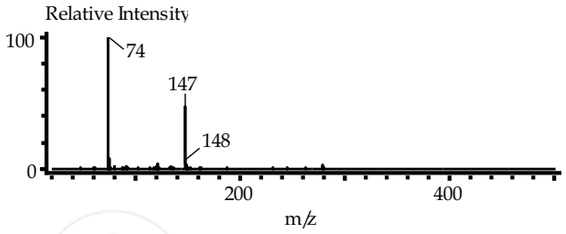

(b) N,N— Dimethyl formamide

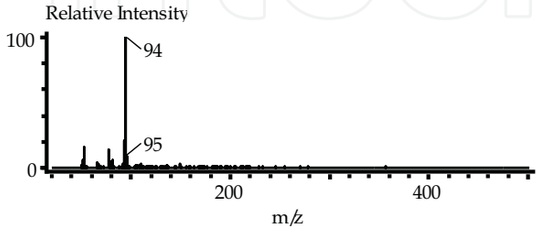

(c) Aniline

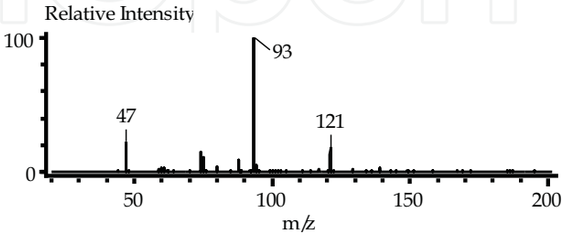

(d) Alcohol

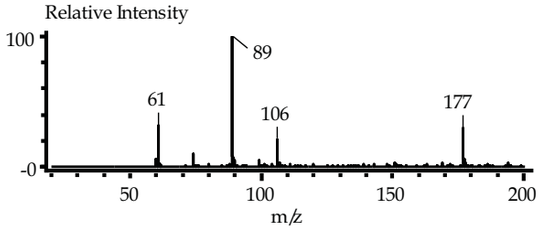

(e) Ethyl acetate

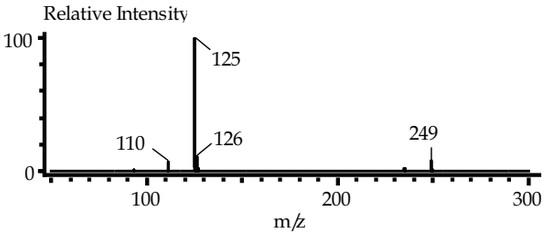

(f) DMMP

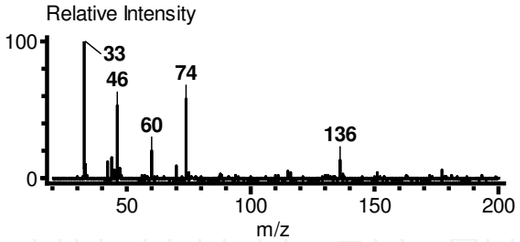

(g) Methanol

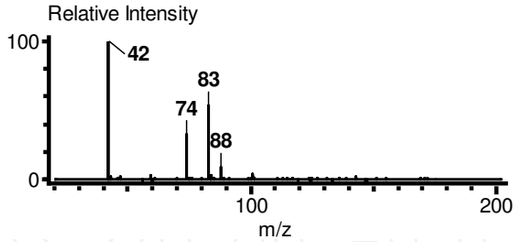

(h) Acetonitrile

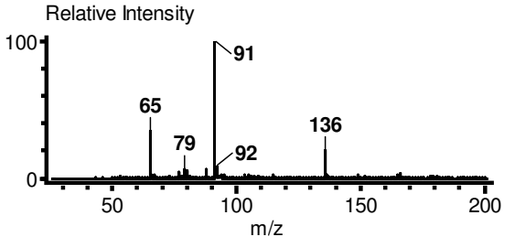

(i) Benzyl alcohol

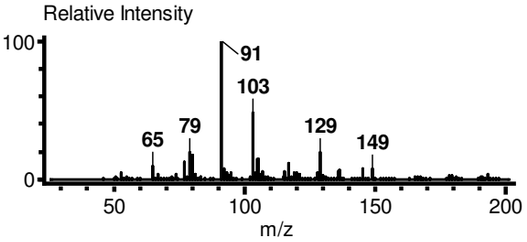

(j) Styrene

Fig. 11. Mass spectrum experimental results under the mode of positive ionisation

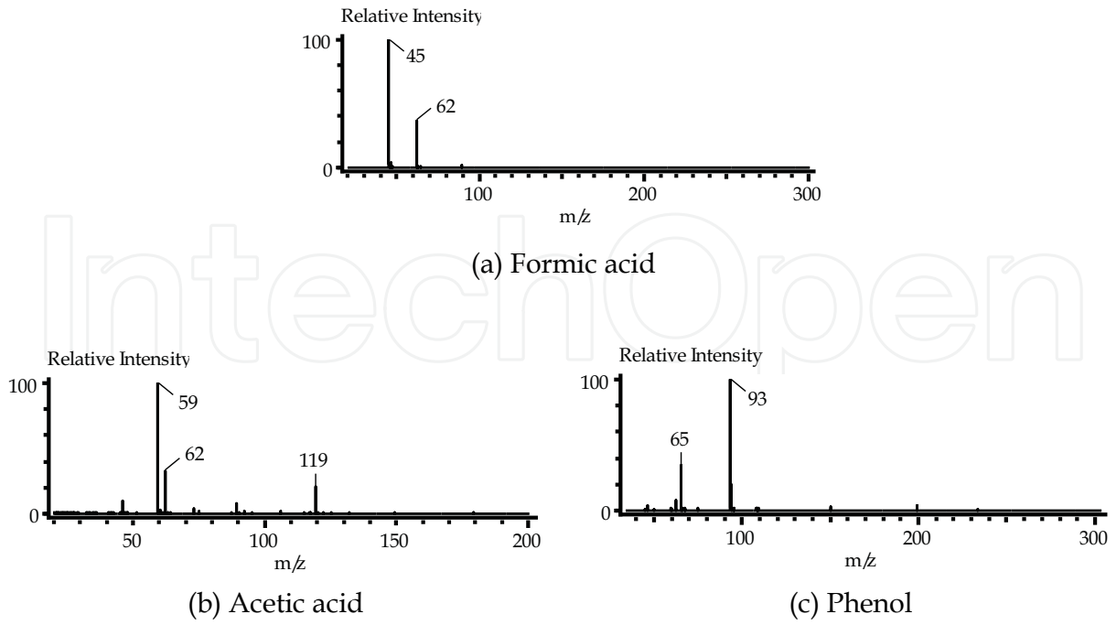

(a) Formic acid

(b) Acetic acid (c) Phenol

Fig. 12. Mass spectrum experimental results under the mode of negative ionisation

Under the mode of negative ionisation, the ions generated are very simple, mainly $[M-H]^-$ and $[M+M-H]^-$, besides, there will be NO_2^- $(M/Z : 46)$ and NO_3^- $(M/Z : 62)$ ions. This is mainly the result of the reaction between nitrogen and oxygen.

4. Design of the high voltage high frequency asymmetric waveform power supply

4.1 Impulse source system based on the power MOSFET

In view of the requirement of the FAIMS system, the FAIMS high-field asymmetric square wave power system is composed of six parts: (1) Signal generator, (2) High speed switch, (3) High voltage direct power supply, (4) High pass filter, (5) Automatic scan and collection of the compensation voltage and (6) Computer. The operation principle block diagram of the high-field asymmetric square wave radio frequency power supply system in FAIMS design is shown in figure 13.

Through electrical isolation and power level conversion, the frequency of output, duty ratio and PWM signal with variable dead band of the signal generator controls the high speed switch of the inverter circuit to generate the high voltage and high frequency square wave impulse output. Controlled by the signal generator, the high voltage direct current power supply provides the high voltage direct current signal for the high speed switch, through which the high voltage and high frequency square wave impulse output are generated. After the square wave impulse output is filtered through the high pass filter, the asymmetry waveform voltage signal output with the same positive and negative area is realised.

In the automatic scan of the compensation voltage, the signal generator is used to control the digital to analog conversion of DAC, and magnify the signal, realising the automatic scan of the compensation voltage of the saw tooth wave. In view of that the radio frequency high voltage side on the electrode plate of the drift region interferes with the low voltage side of the compensation voltage, we realise the electrical isolation between high voltage and low

voltage with the inductance and resistance network, when superposing the compensation voltage onto the drift region. Through voltage attenuation and analog-digital conversion, the influence of the radio frequency can be reduced and accurate collection and detection of the compensation voltage signal can be achieved.

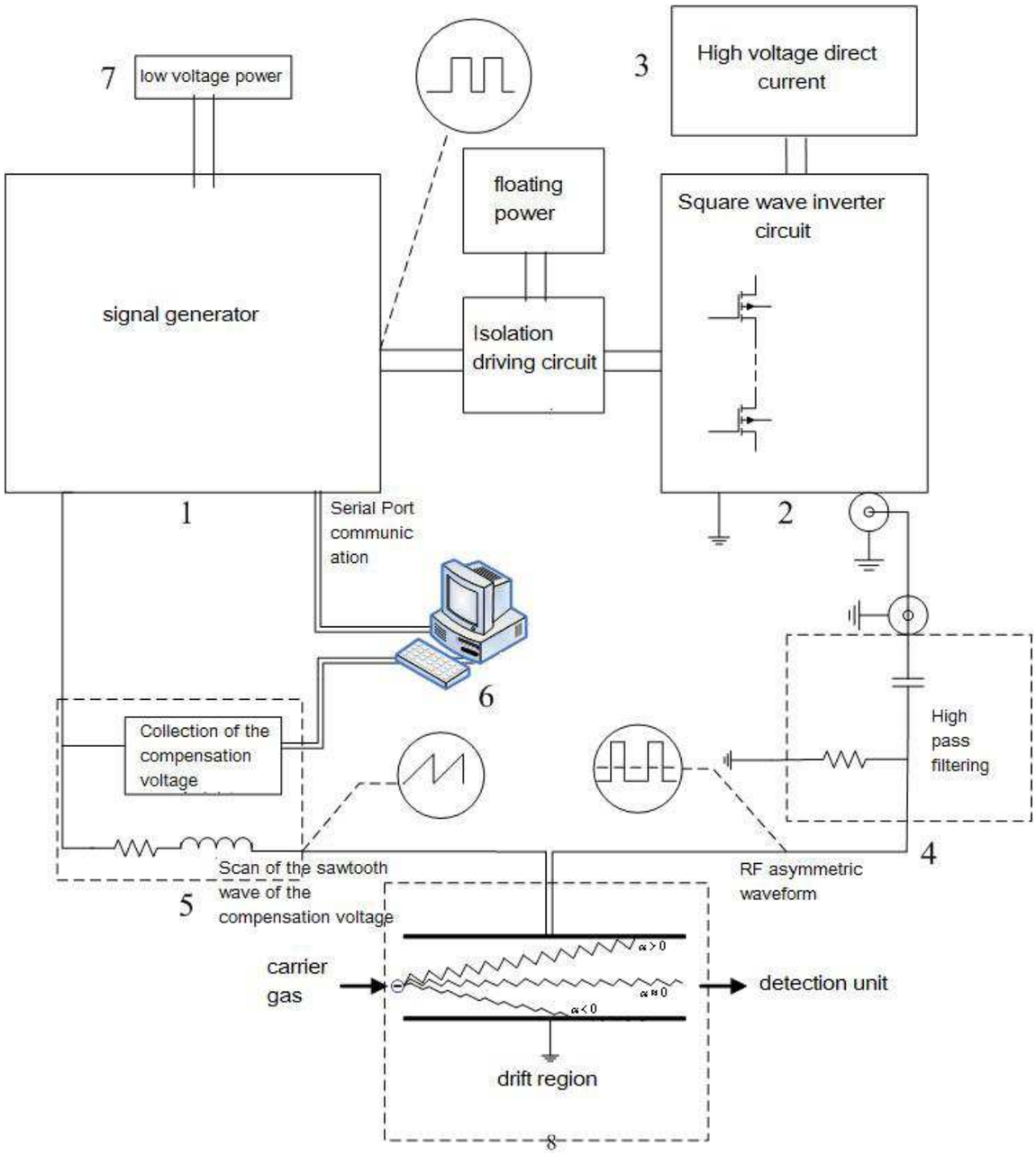

Fig. 13. Square wave RF power supply system block diagram for FAIMS detector

The signal generator is the main control section. It can communicate with the computer through a serial port to adjust the frequency, duty ratio, dead band time and scanning cycle of the compensation voltage on-line.

4.2 Design of each unit circuit in the impulse source system

4.2.1 Realisation of the automatic scanning signal of the compensation voltage

The scanning range for the compensation voltage should be -25V ~ 25V. In this circuit, a TI OPA547 high voltage amplifier is used to magnify signals, which is a precise high voltage large current operational amplifier with a wide dynamic voltage range, a high voltage slew rate of 6V/us and a low quiescent current. When it is provided with a single power supply, the maximum working voltage is 60V. When it works with a double power supply, the working voltage range is ±30V. In the mode of double power supply, the maximum voltage of the maximum input and output signal is ±27V.

4.2.2 Research and design of collection of the compensation voltage

(1) Requirements for collection of the compensation voltage

In order to get the synchronous values of the compensation voltage with the micro current collected by a Faraday Cup, the minimum step of the compensation voltage must be 0.1V. The compensation voltage should be collected at high precision because the amplitude of the compensation voltage is wide: -25V ~ 25V, and the usual collection circuit is CMOS or TTL, which requires collection of the voltage after voltage attenuation. The minimum precision should be 0.4%. Besides, there is high frequency interference and noise from the high voltage and high frequency signal in the drift region, so the interference and noise must be blocked to ensure the accuracy of collecting the compensation voltage. The connection method of the compensation voltage in the actual experiment is shown in figure 14.

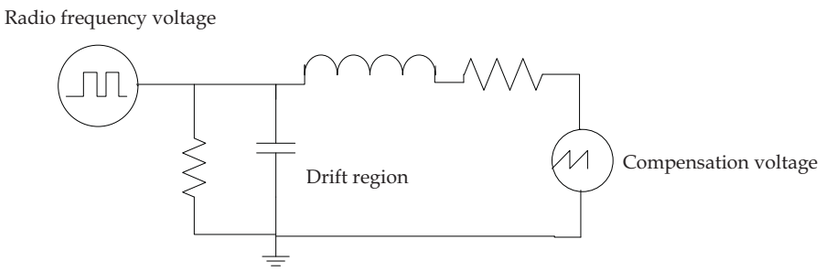

Fig. 14. Compensation voltage connection diagram

(2) Design of the compensation voltage collection

The following two methods are used to control noise: isolation and filter.

1. Isolate the ground of the drift region and the ground of the collection circuit with a bead or Zero Ohm Resistor, to avoid the influence of the noise generated by the high speed switch in the drift region of the collection circuit.
2. Convert the attenuated signal from analog to digital with a high-precision, low noise and low drift double-integral A/D converter, in which an integrator and voltage comparator are used. A double-integral A/D converter has a strong noise control with a mean value of Zero and a high stability, which is a good method to block interference and noise. The results show that when the radio frequency voltage is greater than 300V, the maximum relative error voltages of the compensation voltage will not exceed 4mV, and the measuring accuracy is 0.16%. It shows that in the second plan the compensation voltage can be accurately collected under the interference of the radio frequency, which meets the requirements of the system.

4.2.3 Structure optimisation of the half bridge inverter circuit

To solve the problems in the half-bridge inverter circuit, the circuit structure has been optimised. Figure 15 shows the basic principle diagram of the optimised half bridge inverter circuit. The working principle of the circuit is that: under the control of the driving circuit, the S1 and S2 switches take turns to turn on and generate a high voltage square signal, and then the asymmetric waveform is produced through the C3 and R3 network.

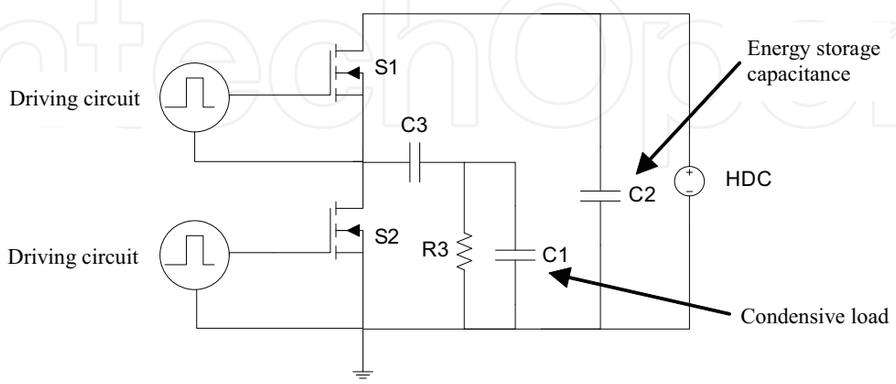

Fig. 15. Basic principle block diagram of the optimised half bridge inverter circuit

Compared with the structure of the half bridge inverter, the following parts have been optimised:

1. To realise a high frequency steep pulse square-wave output. When the frequency of the switch increases, the pulse wave form quality will always change. So we chose a new MOSFET with a low stray parameter, high switching frequency and a short time for rising and falling for wider application.
2. As for the problems of the series MOSFET switches with incomplete synchronisation, we have replaced the two MOSFET with single MOSFET with higher bearing voltage and heat dissipation as the single arm series switching power devices.
3. As for the problems in adjustment of the compensation voltage, we have analysed the generation principle of the square wave, and achieve automatic generation of the asymmetric waveform. The FAIMS asymmetric square waveform is shown in figure 7, in which it can be considered that the average value of the wave in one cycle is zero. Writing the square into a Fourier series expansion:

$$\begin{aligned} f(t) = A_{\max}\{\alpha + \frac{2}{\pi}[2\sin(\alpha\pi)\cdot\cos(\omega_1 t) \\ + \frac{1}{2}\sin(2\alpha\pi)\cdot\cos(2\omega_1 t) \\ + \frac{1}{2}\sin(3\alpha\pi)\cdot\cos(3\omega_1 t) + \cdots\} \\ = \alpha A_{\max} + \frac{1}{\pi}A_{\max}\sum_{n=1}^{\infty}\sin(n\alpha\pi)\cdot\cos(n\omega_1 t) \end{aligned} \tag{15}$$

Where α is the duty ratio of the square wave, $\alpha A_{\max}$ is its direct current component, and the other sine and cosine parts are the components of the alternating current.
The average value of the square wave in one cycle is:

$$A_{av} = \frac{1}{T}\int_0^T f(t) = \alpha A_{\max} \tag{16}$$

We can see from the above formula that the average value of the square wave is the component of its direct current. So after filtering out the DC component in the square wave, we can obtain the asymmetric positive and negative square waves with the same area.
It is required by the FAIMS system that the power consumption and the volume is small. In view of the above advantages and disadvantages of the inverter circuit, we select the half-bridge structure as the inverter circuit, and optimise the half-bridge inverter circuit to achieve a high frequency of non-symmetric square wave outputs.

5. Ion detection

5.1 Design of the micro Faraday cup

MEMS Faraday cup has got a glass - silicon - glass layer structure (as shown in figure 16). The gas route of the Faraday cup is formed with upper glass, lower glass and silicon chips. The middle layer adopts the low resistivity silicon material, the resistance of which is 0.0001 ~ 0.0009Ω·m, to achieve good conductive properties. When the ions collide with the surface of the low resistivity silicon, the ions are neutralised to achieve the drift of the charge to the low resistivity silicon. Through the current collected from low resistivity silicon, the ion beam intensity can be measured. The sensitive electrode of the Faraday cup is composed of dozens of silicon columns. The array arrangement has formed a number of fine gas routes in the sensitive electrodes. When the ions go into the Faraday cup, driven by the carrier gas, they will collide many times with the silicon column in complex micro-channels, and eventually be captured by the sensitive array. The ion signal captured will be educed by the electrode on the glass and read out from the sensitive ammeter.

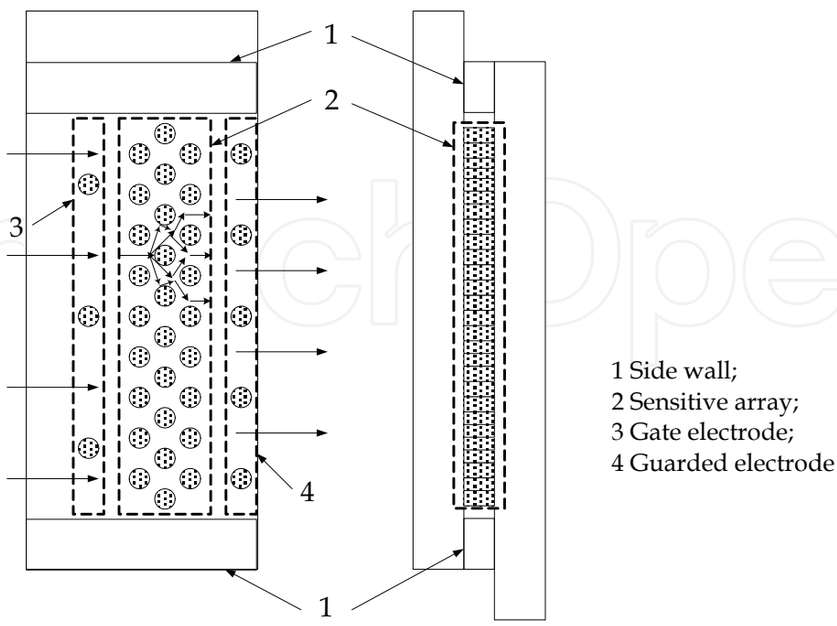

Fig. 16. Structure of the MEMS Faraday cup

For the current signal to be detected, the requirement of the system on the contact resistance characteristics of the silicon and the metal wire is not very high, and it reduces the requirement on the processing of the chips. A gate electrode is set on the front of the sensitive array gas route. The gate electrode is composed of several silicon columns of diameter 200 μm. The gate electrode of low-resistivity silicon is used with a certain voltage. The presence of the gate electrode will bring about a loss of ion signal, resulting in a decrease of sensitivity of the chip, but it can reduce the induced signal before ions reach the sensitive array.
Compared with the traditional Faraday cup, there are advantages in this micro Faraday cup array:

1. The sensitive electrode adopts the array design:
   a) To expand the contact area of the gas with the sensitive electrode
   b) As lots of micro gas flow channels are formed, it is in favour of the disturbance of the stable flow field after the gas goes into the sensitive array, making the ions in the gas more easily collide with the sensitive electrode, reducing the loss of the ion signal
   c) Due to the presence of the micro-flow channel, the carrier gas can carry ions through the sensitive electrodes to achieve ion signal collection. Compared to the electric field drive method, the gas drive approach eliminates the driving electrode and associated power supply so that the structure of the Faraday cup is simpler.
2. The gate electrode, the shielding electrode and conductive shielding wall can provide good shielding for the sensitive electrode, improving the detection limit of the Faraday cup.

5.2 Simulation of a micro Faraday cup

In the FAIMS system, the ion signal is very weak (pA level), and it is easily influenced by human body static electricity and electromagnetic waves in the environment, which brings a critical requirement on the shielding performance for the Faraday cup. The drift region will be applied on the radio frequency voltage, which is a great noise for the detection environment of the Faraday cup. The coupling capacitance of the drift region and the sensitive electrode of the Faraday cup can be used to measure the level of the noise of the electric field on the sensitive electrode of the Faraday cup. We have analysed the coupling capacitance of different structures of the MEMS Faraday cup from an ANSYS simulation, and done the theoretical calculation at the condition whether there is a side wall grounded.
Modelling: When modelling, the MEMS Faraday cup has been simplified. The sensitive electrode of the Faraday cup can be simplified as a rectangular solid conducting block, and the shielding electrode can be simplified as a rectangular solid bar. The air boundary of the Faraday cup is simulated as the outermost shield shell, which is grounded.
Network partitioning: The tetrahedron is divided with smartsize 1 and amesh.
Material and unit: There is only air for dielectric materials, with a relative dielectric constant of 1. The unit adopts the solid122 electromagnetic field solid unit.
Simulation results: Through simulating the coupling capacitance of the sensitive electrode and the drift region in the MEMS Faraday cup, it can be found that the side wall of the MEMS Faraday cup and the shielding electrode are very useful in reducing the radio frequency noise in the drift region. It can be found that through comparing the results of the models c and d, the coupling capacitance will fall a little when the back shielding electrode is added, but the total effect remains the same. In the experiment, the shielding case of the MEMS Faraday cup should be as close as possible to the Faraday cup.

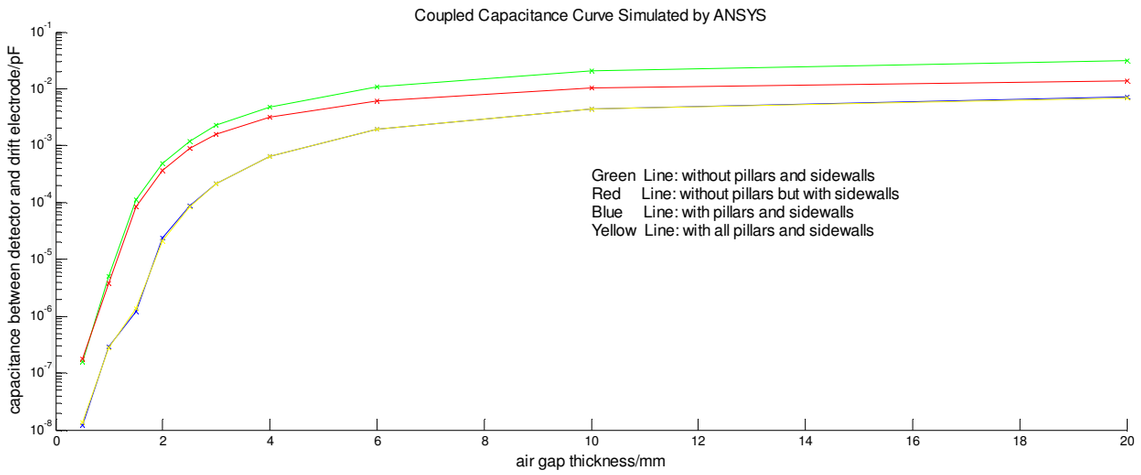

Fig. 17. Coupled capacitance of the drift region and the Faraday sensitive electrode under different conditions. Note: The air gap refers to the distance of the drift region away from the outer edge of the model, that is the space of the MEMS Faraday cup away from extra shield case.

When the sidewall is not grounded, the noise led into the detection circuit through the coupling capacitance between the drift tube and the sensitive electrode is very low. The noise is mainly led into the detection circuit through the sidewall. The equivalent noise generation circuit is shown in figure 18.

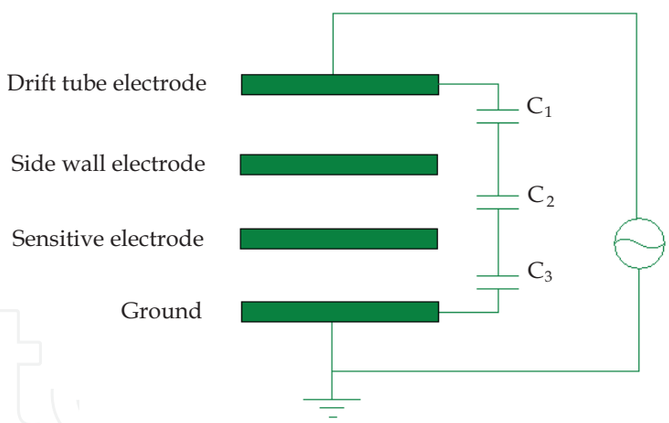

Fig. 18. Circuit model simplified with the side wall non-grounded

The noise voltage on the sensitive electrode is

$$U_d = \frac{1/C_3}{1/C_3 + 1/C_2 + 1/C_1} U \tag{17}$$

When the airgap thickness is 2 mm, $C_1 = 0.2pF$, $C_2 = 0.205pF$ and $C_3 = 0.84pF$ are obtained from the ANSYS simulation result of model c, so

$$U_d = \frac{1/C_3}{1/C_1 + 1/C_2 + 1/C_3} U = \frac{1/0.84}{1/0.2 + 1/0.205 + 1/0.84} U = 0.107U$$

where U_d is the noise voltage on the sensitive electrode, U is the noise source in the drift tube, C_1 is the capacitance between drift tube and the sidewall, C_2 is the capacitance between the sidewall and the sensitive electrode, C_3 is the capacitance between the sensitive electrode and the ground.

When the sidewall is grounded, the noise in the drift tube is mainly led into the detection circuit by electromagnetic field coupling through the coupling capacitance between the drift tube and the sensitive electrode. The equivalent noise generation circuit is shown as figure 19. The noise voltage on the sensitive electrode is

$$U_d = \frac{1/C_3}{1/C_3 + 1/C_4} U = \frac{C_4}{C_4 + C_3} U \tag{18}$$

When the airgap thickness was 2 mm, $C_4 = 0.21 \times 10^{-4} pF$ was obtained from the ANSYS simulation result of model c, so

$$U_d = \frac{C_4}{C_4 + C_3} U = \frac{0.21 \times 10^{-4}}{0.21 \times 10^{-4} + 0.84} U = 2.5 \times 10^{-5} U$$

where C_4 is the coupling capacitance between drift tube and the sensitive electrode, C_5 is the capacitance between drift tube and the ground.

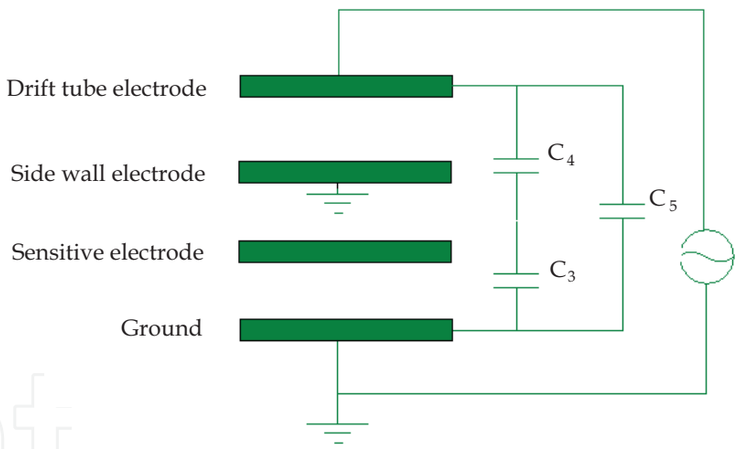

Fig. 19. Circuit model when the side wall is grounded

By comparing the both results, the sidewall grounding can greatly decrease the interference from drift tube on the sensitive electrode.

5.3 Micro Faraday cup technology

The design of the MEMS Faraday cup is shown in figure 16. We have designed the MEMS process and the latter welding process of the MEMS Faraday cup according to the structure of the MEMS Faraday cup and the technological characteristic of the MEMS production line. The thickness of the silicon chip is 200μm, which is n type of 3 inch disk with a specific resistance of 0.0001~0.0009Ω·m, the glass plate is a 3 inch disk, the thickness of which is 500μm. The MEMS Faraday cup chip fabricated is shown as figure 20.

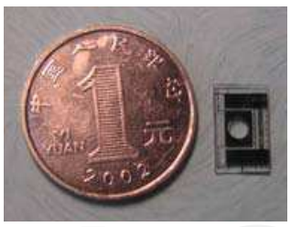

Fig. 20. Photo of the MEMS Faraday cup

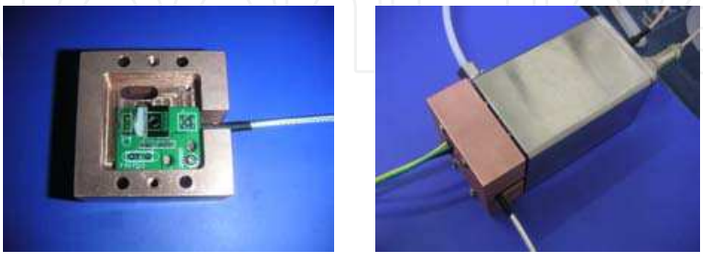

Fig. 21. Photos of the MEMS Faraday cup packaged

5.4 Testing of the micro Faraday cup

For the MEMS Faraday cup chip packaged with PCB, a base should be fabricated to realise a reliable connection between the MEMS Faraday cup and the ion source. The base is made of red copper, which can effectively shield the noise from the environment. The photos of the red copper shielding base, assembled MEMS Faraday cup and the ion source are shown in figure 21.

In order to test the performance of the MEMS Faraday cup, the chip is tested with KEITHLEY237. In this experiment, the carrier gas is nitrogen gas and the sample is acetone, the concentration of which is about 100ppm. The experimental system is shown in figure 22.

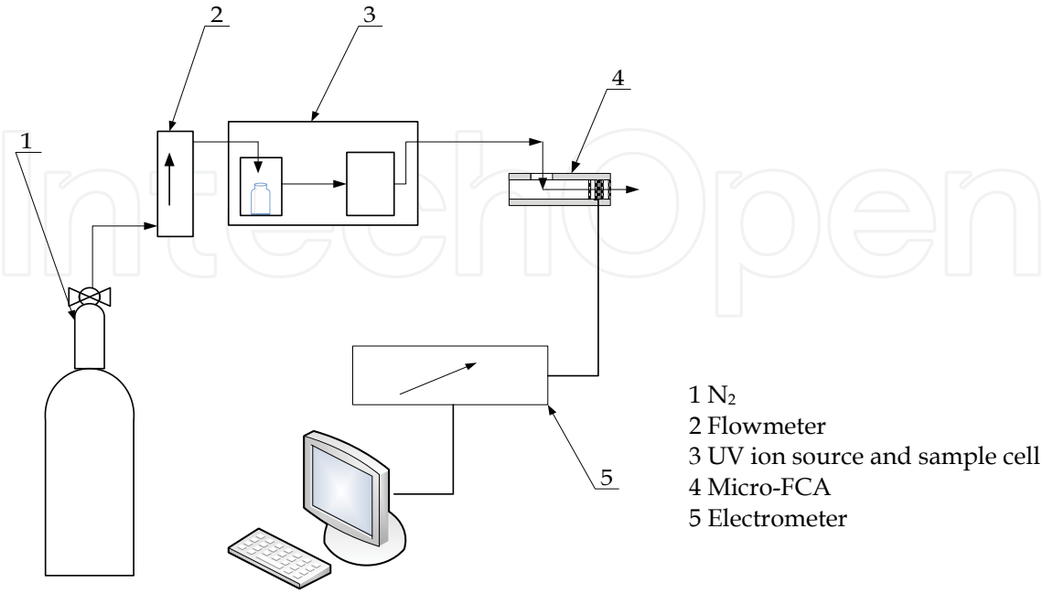

Fig. 22. Experimental apparatus of the MEMS Faraday cup

(1) Ion collection experiment with the MEMS Faraday cup

In the experimental system of figure 22, the carrier gas flow is adjusted to 100L/h. We make the comparison of the ion collection results among the chips of the MEMS Faraday cup with different structural parameters. Through comparison of the signal, the absorption efficiency of the MEMS Faraday cup with different structural parameters is evaluated.

Figure 23 shows a typical ion signal curve collected by the MEMS Faraday cup. This means that the signal of the MEMS Faraday cup is stable, which can work in the atmospheric environment, and is completely capable of detect ion.

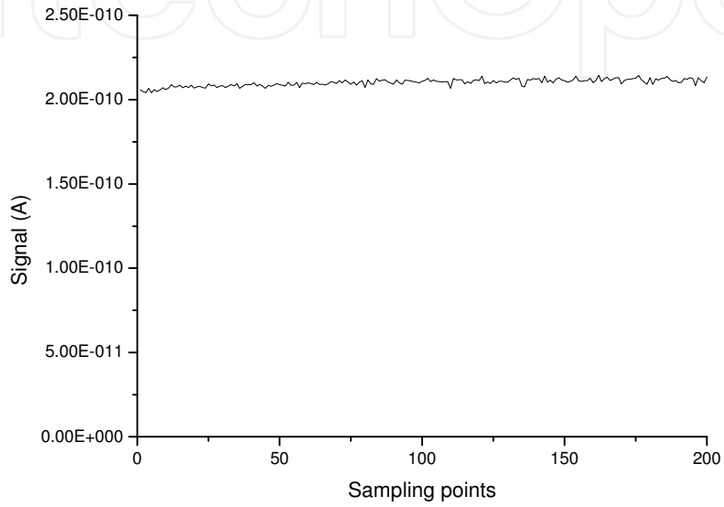

Fig. 23. Ion signal curve received by the MEMS Faraday cup

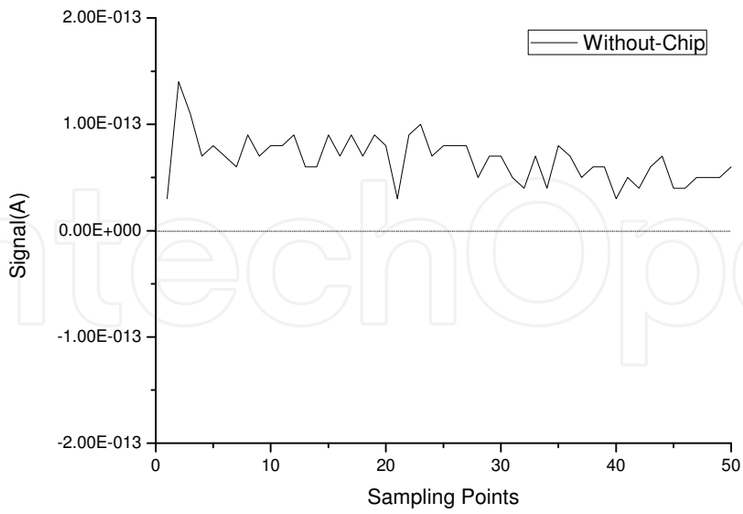

Fig. 24. Noise in the body of KEITHLEY

(2) Anti-interference experiment

Shut off the carrier gas and apply the radio frequency voltage (the maximum is 300V and the frequency is 200kHz) between the upper and lower electrodes in the front of the micro

Faraday cup. We test the influence of different shielding methods and different chip structures on the ability of anti-interference.

First of all, in the case without the chip, we tested the background noise of the system with KEITHLEY current testing module, as shown in figure 24. The average value of the noise curve is 67.2fA. The offset current may be from the interference source in the environment or the offset of the instruments. We have found biased data always from 40 to 80 fA in many measurements. In the following data treatment, the biased current should be subtracted from the original data.

1) The influence of RF electric field on the noise under different connection ways

The experimental results are shown in figure 25. In this experimental system, we found the influence of the RF electric field and the copper shielding base on the noise of the chip is not obvious. The level of the noise is about 0.1pA. It means that under this experimental system setup there is no influence of different connections on the noise of the chip.

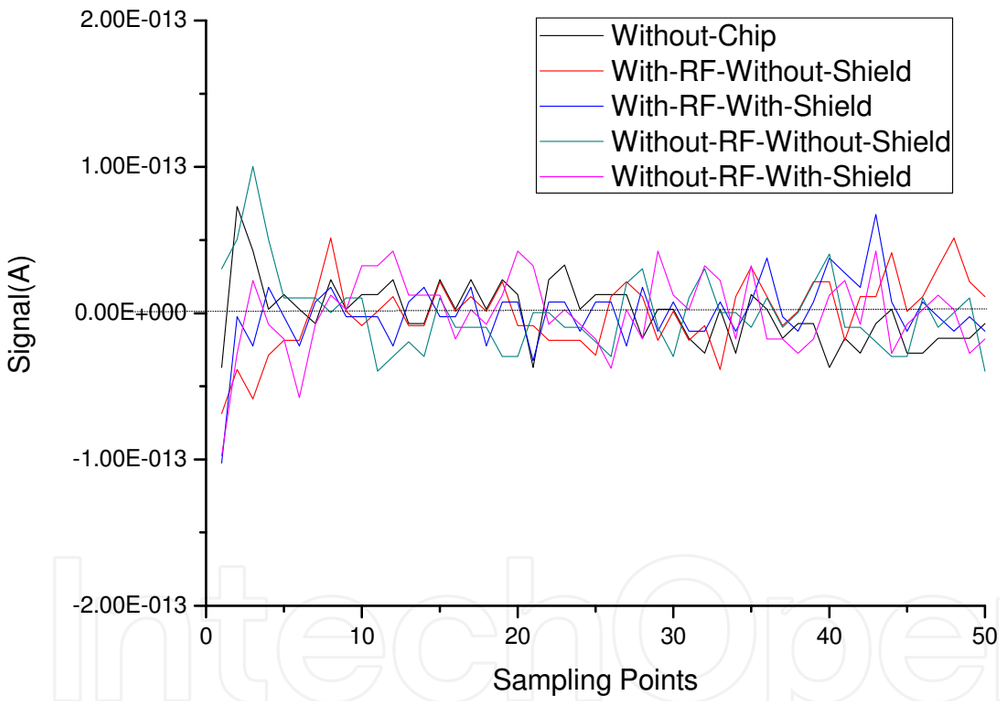

Fig. 25. The noise level of the same chip under different connections. Note: corresponding biased current has been subtracted in each curve.

2) Influence of different chip structures on the noise

Connecting ways and RF electric fields have no influence on the noise, so we have conducted the noise test for the chip with different structural parameters, without the copper shielding base and RF electric field.

It can be seen from the figure 26 that in this experimental system, whether or not the gate electrode in the chips exists or the side wall of the drift regions and the side of the Faraday cup are separated has no influence on the noise.

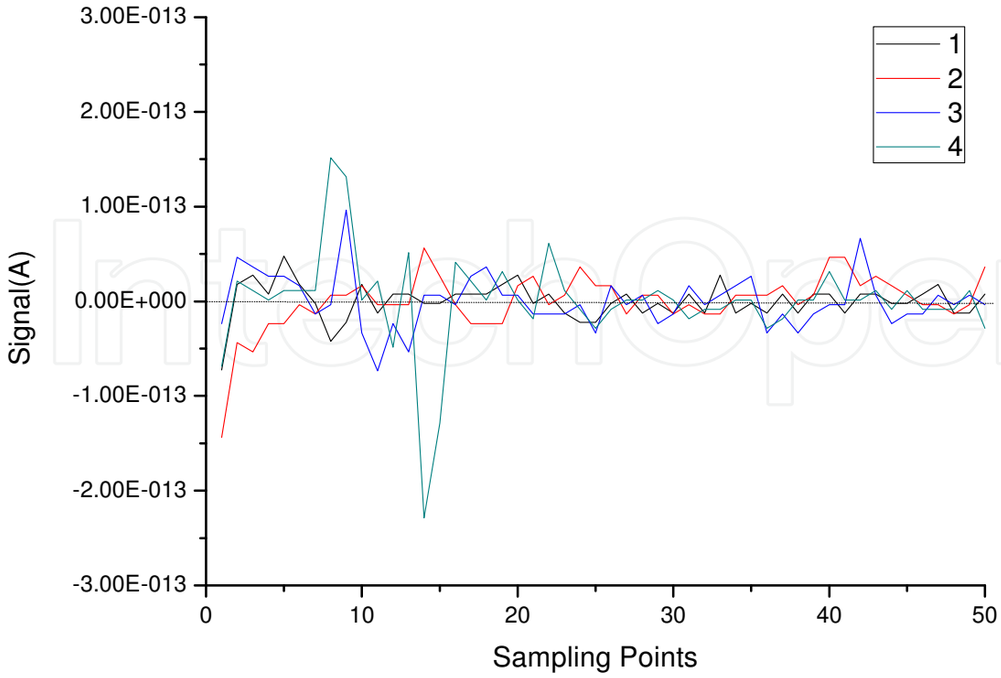

Fig. 26. Noise level with different chip structures. Note: 1) corresponding biased current has been subtracted in each curve 2) Structure1: no gate electrode, the side wall of the drift region is separated with the silicon side wall of the Faraday cup 3) Structure2: gate electrode with three silicon columns, the side wall of the drift region is separated with the silicon side wall of the Faraday cup 4) Structure3: gate electrode with five silicon columns, the side wall of the drift region is separated with the silicon side wall of the Faraday cup 5) Structure4: gate electrode with five silicon columns, the side wall of the drift region is connected with the silicon side wall of the Faraday cup

6. Sample analytical experiment

6.1 Experimental system of FAIMS chip

The experimental system of FAIMS is composed of a sample injection unit, ion source, FAIMS chip, square wave radio frequency power, and data collection unit, as shown in figure 27. The sample injection unit contains the nitrogen tank, flowmeter and sample cell. The ion source is composed of the ion source power and a 10.6eV ultraviolet lamp. The data collection unit contains amperometer, compensation voltage data collection card and computer.

6.2 Influence of the changing of the square wave radio frequency voltage amplitude on the sensitivity of FAIMS

We take absolute ethyl alcohol as the sample in this experiment. The flow velocity of the carrier gas is 0.8L/min in this experiment, the square wave radio frequency voltage frequency is 2MHz, and the duty ratio is maintained at about 30%. The amplitude of the square wave radio frequency voltage is increased to 380V from 220V, at 20V intervals. When the compensation voltage automatically scans in the scope of +10V~-10V, the FAIMS spectrogram of alcohol is shown in figure 28. In figure 28, the ion peak near the compensation voltage 0V is the background noise signal, which will be ignored in the following analysis.

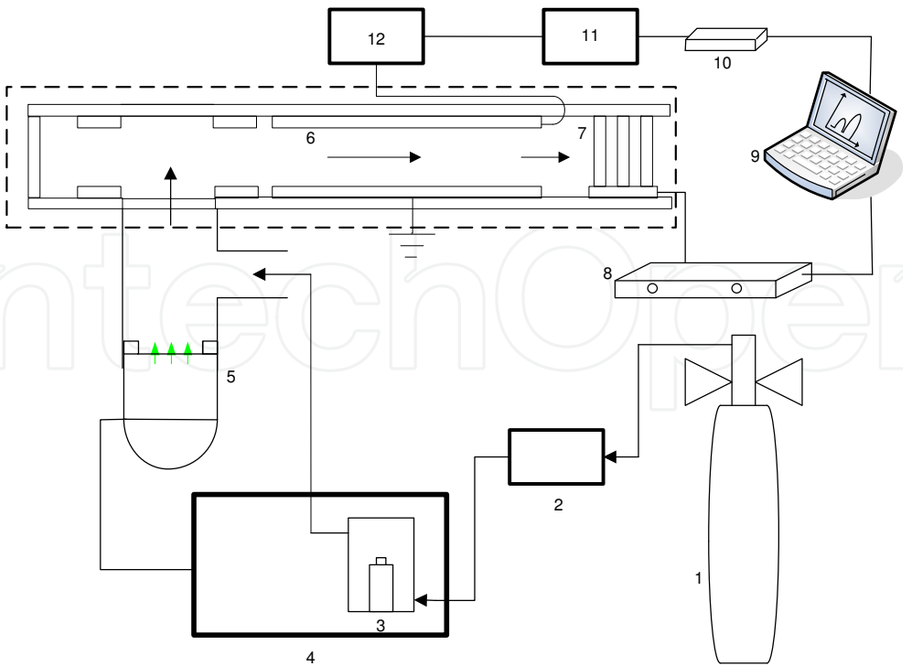

1 Nitrogen tank, 2 Flowmeter, 3 Sample cell, 4 Ion source power, 5 Ultraviolet lamp, 6 Drift region, 7 Column array micro Faraday cup, 8 Amperometer, 9 Computer, 10 Collection card, 11 Compensation voltage, 12 Square wave radio frequency voltage

Fig. 27. FAIMS chip experimental system block diagram

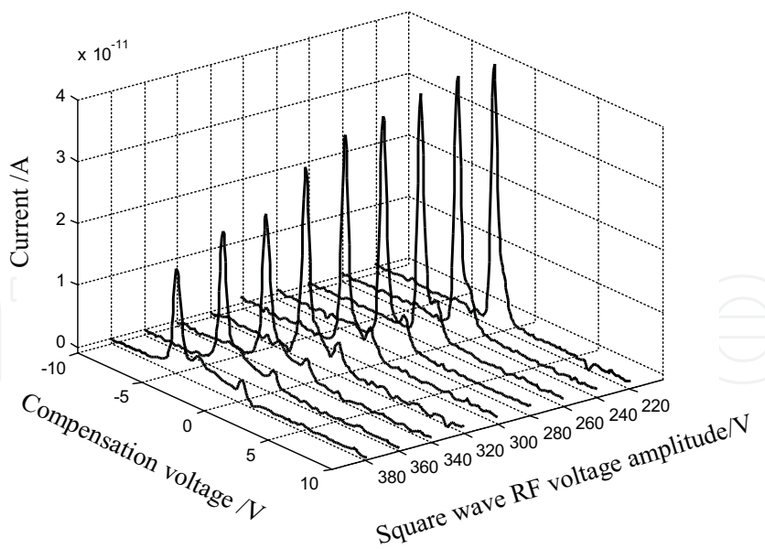

Fig. 28. The FAIMS spectrogram of alcohol corresponding with different radio frequency voltage amplitude

It can be seen from figure 28 that in the FAIMS system when the amplitude of the radio frequency voltage increases, the intensity of the ion peak signal detected will be lower. This is oppose to the influence of the voltage amplitude on the intensity of the ion peak in the

IMS system. The relation between the square wave radio frequency voltage amplitude and the ion peak signal current is shown in figure 29. With an increase of the voltage amplitude, the current will gradually decrease to 16.1pA at 380V from 41.7pA at 220V.

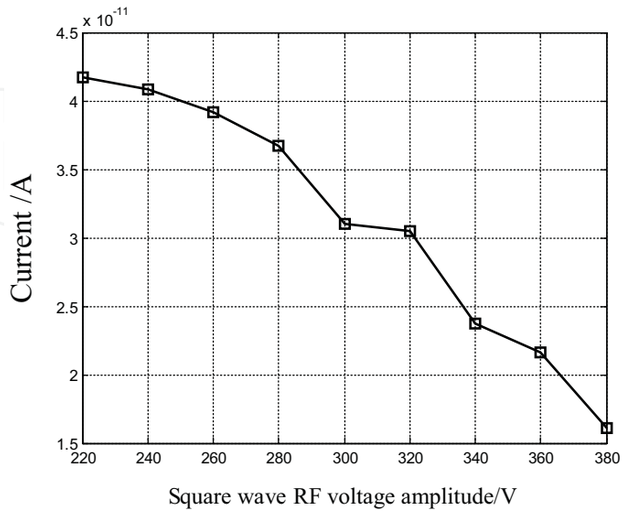

Fig. 29. Influence of the amplitude of the square wave RF voltage on the peak of the ethanol

For substances with small molecules such as ethanol, the ion mobility K will increase when the amplitude of the voltage V_H increases. $\alpha(E/N)$ will also increase when the amplitude of voltage V_H increases, and so will the compensation voltage V_{co} and resolution R. Figure 30 and figure 31 show the curve of compensation voltage and the resolution of the ethanol with the radio frequency voltage, respectively. It can be seen from the figures that the compensation voltage and the resolution are increased to -4.86V and 6.57 at 380V from -0.64V and 1.12 at 220V, respectively. The changing trend fits closely with the theoretical analysis.

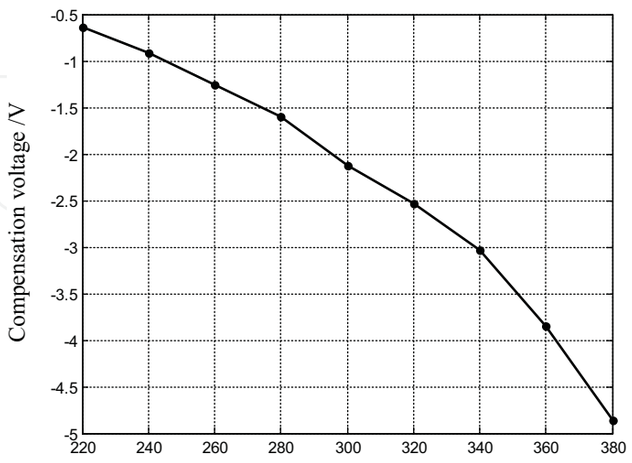

Fig. 30. Relation curve between the compensation voltage and the amplitude of the square wave radio frequency voltage

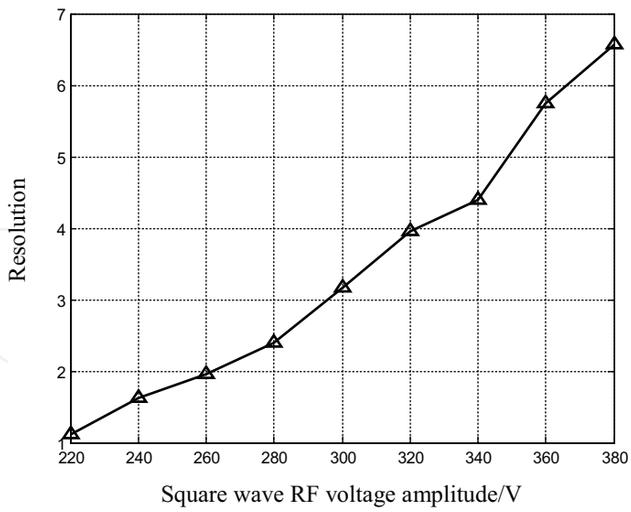

Fig. 31. Relation curve between the resolution and the amplitude of the square wave radio frequency voltage

6.3 Influence of the radio frequency voltage amplitude, frequency and flow velocity of the carrier gas on the FAIMS detection result of 2- pentane

(1) Influence of the amplitude of the voltage

If the flow velocity of the carrier gas is kept at 1L/min, the square wave RF voltage frequency is 2MHz, and the duty ratio is 30%, when the amplitude of the square wave radio frequency voltage increases from 220V to 320V at 20V intervals we can obtain the FAIMS spectrogram as shown in figure 32. We can see from figure 32 that with an increase in the amplitude of the square wave radio frequency voltage, the compensation voltage value (absolute value, same as below) will increase and the ion signal intensity will fall.

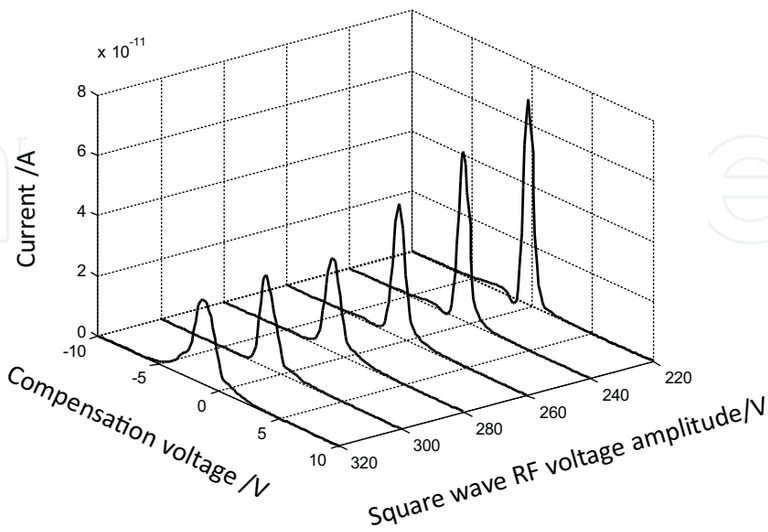

Fig. 32. The FAIMS spectrogram of 2- pentane corresponding to different square wave RF voltage amplitudes

The ion mobility of the 2-pentane will increase with increasing electric field intensity (Papanastasiou et al., 2008). So with increasing voltage amplitude, the amplitude of the ion will increase under the effect of the high electric field, the net displacement in one cycle will increase, and the compensation voltage for reverse compensation on the net displacement will also increase. On the other hand, the diffusion coefficient of the ion will increase with increasing ion mobility, so the ion loss caused by diffusion will increase while the ion signal intensity falls.

(2) Influence of the frequency

The frequency of the square wave radio frequency voltage is an important parameter of FAIMS, the value of which has directly affected the passing efficiency of ions in the drift region. Under the condition that the square wave radio frequency voltage amplitude is 320V, the duty ratio is 30% and the flow velocity of the carrier gas is kept at 1L/min, the FAIMS spectrogram of 2-pentane when the frequency is 2MHz, 1.75MHz, 1.5MHz and 1.25MHz is as shown in figure 33. We can see from figure 33 that the ion signal intensity will decrease with decreasing frequency. It drops from 28pA at 2MHz to 9.43pA at 1.25MHz, while the compensation voltage *Vc* stays the same at -1.33V. At the same time, the FAIMS spectrogram will become narrower as the frequency decreases, namely the resolution increases. The reason is that the decreasing frequency will increase the cycle, which increases the amplitude of ions, making the effective width smaller. In this way the ion loss due to collisions with the electrode becomes larger, and the ion signal intensity decreases, thus the resolution increases. It was shown from theoretical formula that the frequency change does not affect the value of compensation voltage (Papanastasiou et al., 2008).

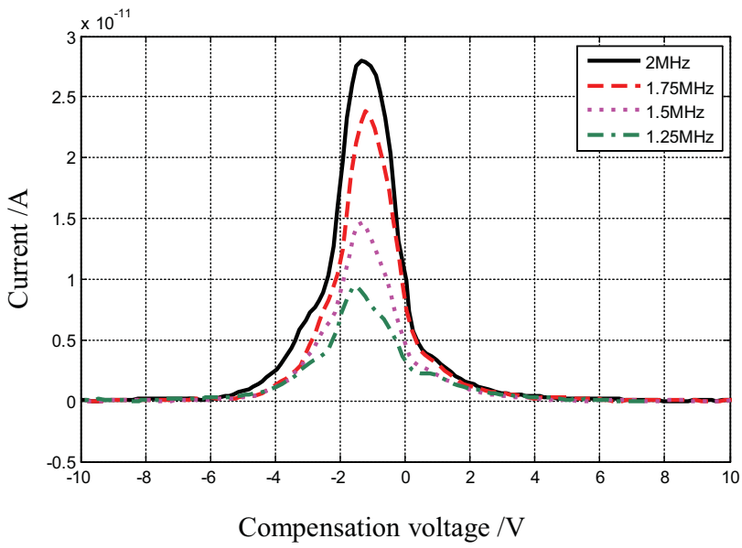

Fig. 33. The FAIMS spectrogram of 2-pentane corresponding with different square wave radio frequency voltages

(3) Influence of the flow velocity of the carrier gas

When the square wave radio frequency voltage amplitude is 320V, the duty ratio is 30%, and the frequency is 2MHz, the flow velocity of the carrier gas increases from 0.6L/min to 1.4L/min. It can be identified from figure 34 that when the flow velocity of the carrier gas

increases, the signal intensity of the ion will increase, while the compensation voltage value *Vc* stays the same at -1.33V. When the flow velocity increases, the FAIMS spectrogram will broaden, namely the resolution is reduced. The increase of the carrier gas velocity makes the time the ion takes to travel through the drift region shorter and the number of movement cycles in the drift region is reduced, so the ion loss due to ion diffusion and neutralisation of the positive and negative ions becomes smaller. But the net displacement in one cycle stays the same so the ion signal intensity is improved, the compensation voltage stays the same, and the resolution is reduced.

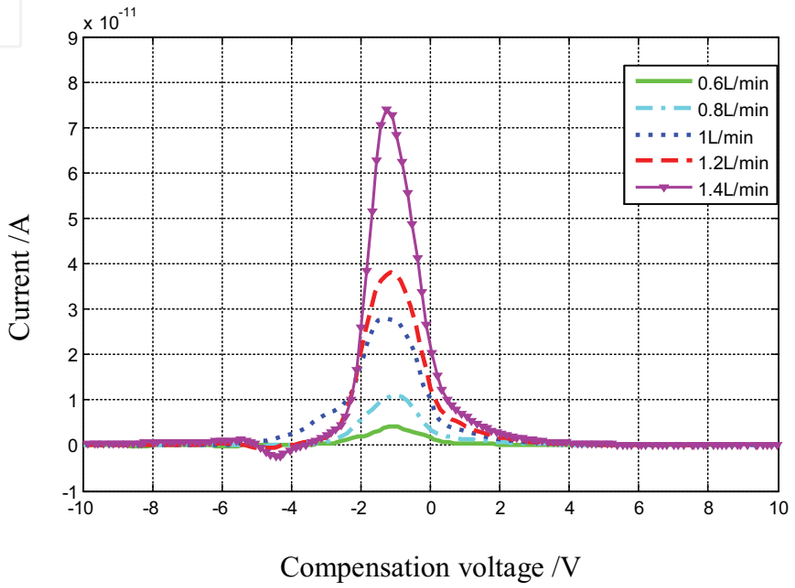

Fig. 34. Influence of the flow velocity of the carrier gas on FAIMS spectrogram

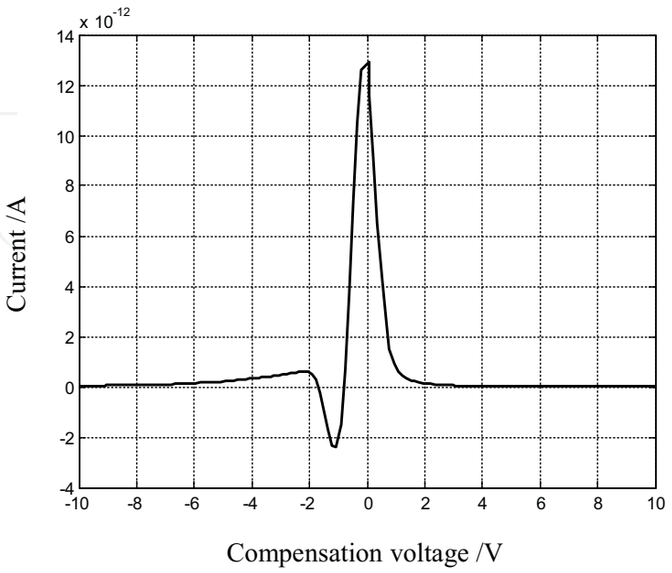

Fig. 35. FAIMS Spectrogram of 0.1ppm acetic acid

6.4 FAIMS chip detection limit experiment

The experimental sample is acetic acid. The sample bottle is sealed with a film with a 160μm diameter hole at its centre, to reduce volatilisation of the sample and acquire a sample of lower concentration. The carrier gas is high purity nitrogen (99.999%), the flow of which is 100L/h. The concentration of the acetic acid is about 0.1ppm through acid base titration with NaOH of known concentration.

The parameter setting in this experiment is as follows: the square wave radio frequency voltage amplitude is 220V, the frequency is 2MHz, and the duty ratio is 30%, the polarisation voltage of the ultraviolet lamp is -150V, the FAIMS Spectrogram of the acetic acid is shown in figure 35.

It can be concluded from figure 35 that a -2.4pA current signal can be obtained with 0.1ppm acetic acid through the FAIMS chip test. It means that the detection sensitivity of the FAIMS chip is high, with which a 0.1ppm acetic acid sample signal can be detected.

7. References

West, C.; Baron, B. & Minet, J. J. (2007). Detection of gunpowder stabilizers with ion mobility spectrometry. *Forensic Science International*, Vol.166, No.2, (March 2007), pp. 91-101, ISSN 0379-0738

Laiko, V. V. (2006). Orthogonal extraction ion mobility spectrometry. *J Am Soc Mass Spectrom*, Vol.17, No.4, (April 2006), pp. 500-507, ISSN 1044-0305

Borsdorf, H.; Nazarov, E. G.; Miller, R. A. (2006). Atmospheric-pressure ionization studies and field dependence of ion mobilities of isomeric hydrocarbons using a miniature differential mobility spectrometer. *Analytica Chimica Acta*, Vol.575, No.1, (August 2006), pp. 76-88, ISSN 0003-2670

Miller, R. A.; Nazarov, E. G. & Eiceman, G. A. (2001). A MEMS radio-frequency ion mobility spectrometer for chemical vapor detection. *Sens Actu A*, Vol.91, No.3, (July 2001), pp. 301-312, ISSN 0924-4247

Miller, R. A.; Eiceman, G. A. & Nazarov, E. G. (2000). A novel micromachined high-field asymmetric waveform-ion mobility spectrometer. *Sens Actu B*, Vol.67, No.3, (September 2000), pp. 300-306, ISSN 0925-4005

Barnett, D. A.; Ells, B. & Guevremont, R. (2002). Application of ESI-FAIMS-MS to the analysis of tryptic peptides. *J Am Soc Mass Spectrom*, Vol.13, No.11, (November 2002), pp. 1282–1291, ISSN 1044-0305

Shvartsburg, A. A.; Smith, R. D. & Wilks, S. A. (2009). Ultrafast differential ion mobility spectrometry at extreme electric fields in multichannel microchips. *Anal Chem*, Vol.81, No.15, (July 2009), pp. 6489-6495, ISSN 0003-2700

Eiceman, G. A.; Nazarov, E. G. & Miller, R. A. (2000). A micro-machined ion mobility spectrometer-mass spectrometer. *Int J Ion Mobil Spec*, Vol.3, No.1, (January 2000), pp. 15-27, ISSN 1435-6163

Guevremont, R.; Purves, R. W. (1999). Atmospheric pressure ion focusing in a high-field asymmetric waveform ion mobility spectrometer. *Rev. Sci. Instrum.*, Vol.70, No.2, (February 1999), pp. 1370-1383, ISSN 0003-46748

Nazarov, E. G.; Miller, R. A.; Eiceman, G. A.; Stone, John A. (2006). Miniature differential mobility spectrometry using atmospheric pressure photoionization. *Analytical Chemistry*, Vol.78, No.13, (July 2006), pp. 4553-4563, ISSN 0003-2700

Shvartsburg, A. A.; Tang, K. & Smith, R. D. (2004). Modeling the resolution and sensitivity of FAIMS analyses. *J Am Soc Mass Spectrom*, Vol.15, No.10, (October 2004), pp. 1487-1498, ISSN 1044-0305

Barnett, D. A.; Belford, M.; Dunyach, J. J.; Purves, R. W. (2007). Characterization of a Temperature-Controlled FAIMS System. *J Am Soc Mass Spectrom*, Vol.18, No.9, (September 2007), pp. 1653-1663, ISSN 1044-0305

Eiceman, G. A.; Tadjikov, B.; Krylov, E.; Nazarov, E. G.; Miller, R. A.; Westbrook, J.; Funk, P. (2001). Miniature radio-frequency mobility analyzer as a gas chromatographic detector for oxygen-containing volatile organic compounds, pheromones and other insect attractants. *Journal of Chromatography A*, Vol.917, No.1-2, (May 2001), pp. 205-217, ISSN 0021-9673

Buryakov, I. A.; Krylov, E. V.; Nazarov, E. G.; Rasulev, U. K. (1993). A new method of separation of multi-atomic ions by mobility at atmospheric pressure using a high-frequency amplitude-asymmetric strong electric field. *Int J Mass Spectrom Ion Processes*, Vol.128, No.3, (October 1993), pp. 143-148, ISSN 0168-1176

Krylov, E. V. (2003). Comparison of the planar and coaxial field asymmetrical waveform ion mobility spectrometer. *Int J Mass Spectrom*, Vol.225, No.1, (February 2003), pp. 39-51, ISSN 1387-3806

Khayamian, T.; Tabrizchi, M.; Jafari, M. T. (2003). Analysis of 2,4,6-trinitrotoluene, pentaerythritol tetranitrate and cyclo-1,3,5-trimethylene-2,4,6-trinitramine using negative corona discharge ion mobility spectrometry. *Talanta*, Vol.59, No.2, (February 2003), pp. 327-333, ISSN 0039-9140

Tabrizchi, M.; Rouholahnejad, F. (2004). Corona discharge ion mobility spectrometry at reduced pressures. *Rev. Sci. Instrum.*, Vol.75, No.11, (November 2004), pp. 4656-4661, ISSN 0003-46748

Jafari, M. T.; Khayamian, T.; Shaer, V.; Zarei, N. (2007). Determination of veterinary drug residues in chicken meat using corona discharge ion mobility spectrometry. *Anal. Chim. Acta.*, Vol.581, No.1, (January 2007), pp. 147-153, ISSN 0003-2670

Khayamian, T.; Tabrizchi, M. (2001). Direct determination of ultra-trace amounts of acetone by corona-discharge ion mobility spectrometry. *Fresen. J Anal. Chem.*, Vol.370, No.8, (August 2001), pp. 1114-1116, ISSN 0937-0633

Papanastasiou, D.; Wollnik, H. & Rico, G. (2008). Differential mobility separation of ions using a rectangular asymmetric waveform. *J Phys Chem A*, Vol.112, No.16, (March 2008), pp. 3638-3645, ISSN 1089-5639

New Perspectives in Biosensors Technology and Applications

Edited by Prof. Pier Andrea Serra

ISBN 978-953-307-448-1
Hard cover, 448 pages
Publisher InTech
Published online 27, July, 2011
Published in print edition July, 2011

A biosensor is a detecting device that combines a transducer with a biologically sensitive and selective component. Biosensors can measure compounds present in the environment, chemical processes, food and human body at low cost if compared with traditional analytical techniques. This book covers a wide range of aspects and issues related to biosensor technology, bringing together researchers from 12 different countries. The book consists of 20 chapters written by 69 authors and divided in three sections: Biosensors Technology and Materials, Biosensors for Health and Biosensors for Environment and Biosecurity.

INTECH
open science | open minds

InTech Europe
University Campus STeP Ri
Slavka Krautzeka 83/A
51000 Rijeka, Croatia
Phone: +385 (51) 770 447
Fax: +385 (51) 686 166
www.intechopen.com

InTech China
Unit 405, Office Block, Hotel Equatorial Shanghai
No.65, Yan An Road (West), Shanghai, 200040, China
中国上海市延安西路65号上海国际贵都大饭店办公楼405单元
Phone: +86-21-62489820
Fax: +86-21-62489821

IntechOpen